ADVANCED FUNCTIONAL MATERIALS

FULL PAPER

DOI: 10.1002/adfm.200800244

Soft Nanopatterning on Light-Emitting Inorganic–Organic Composites**

By *Luana Persano, Sandra Molle, Salvatore Girardo, Antonio A. R. Neves, Andrea Camposeo, Ripalta Stabile, Roberto Cingolani,* and *Dario Pisignano**

In this work we demonstrate the nanopatterning of nanocomposites made by luminescent zinc oxide nanoparticles and light-emitting conjugated polymers by means of soft molding lithography. Vertical nanofluidics is exploited to overcome the polymer transport difficulties intrinsic in materials incorporating nanocrystals, and the rheology, fluorescence, absolute quantum yield, and emission directionality of the nanostructured composites are investigated. We study the effect of patterned gratings on the directionality of light emitted from the nanocomposites, finding evidence of the enhancement of forward emitted light, due to the printed wavelength-scale periodicity. These results open new possibilities for the realization of nanopatterned devices based on hybrid organic-inorganic systems.

1. Introduction

Nanocomposite systems[1] consisting of a polymer matrix filled by inorganic nanoparticles exhibit tailored or improved mechanical,[2] thermal,[3] catalytic[4] or optical [5] properties. In particular, the incorporation of micro- or nanocrystals in conjugated polymers[5a,c,e,g,i] allows one to exploit the wide tunability, ease of processing and structural flexibility of organics, together with the optical and thermal stability of inorganic light-emitting fillers for the specific design of broadly tunable optically active materials. In our previous work,[5i] we studied how the organic–inorganic interaction can be often described through a dipole-surface scheme, determining the characteristic activation energies of the exciton recombination routes in the nanocomposite. However, a crucial issue for the realization of nanocomposite-based optoelectronic devices still is the development of suitable lithographic technologies for wavelength-scale (sub-micrometer) patterning. To date, patterning of hybrid nanocomposites embedding luminescent nanocrystals has been accomplished by electron-beam,[6] optical[7] and imprint lithographies,[8] by exploiting optically inert matrices such as methacrylate polymers and copolymers,[6,7b,8b] epoxy-based photoresists[7a] and titania pre-polymers.[8a] Instead, notwithstanding the great importance of these materials for both fundamental studies and applications,[5a,c,e,g,i] nanopatterning of composites with nanocrystals incorporated in light-emitting organics is basically unexplored, likely due to the more difficult processability induced by the limited solubility and relatively poor thermoplastic behaviour of many conjugated polymers. Here we demonstrate the nanopatterning of such an important class of composites by soft moulding (SM) lithography, achieving resolutions up to a few hundreds of nanometres on several light-emitting polymers embedding zinc oxide particles [molecular structures (**1**–**4**) and crystalline structure of ZnO displayed in Fig. 1].

2. Results and Discussion

The SM, or capillary force lithography,[9] combines procedures and advantages of soft[10] and nanoimprint[11] methods. A scheme of our process is shown in Figure 2a–d. Once an elastomeric mould is put in contact with the surface of the nanocomposite film (Fig. 2a), the overall system is driven above the softening temperature of the polymer matrix (Fig. 2b). Widely employed in soft lithographies,[10] low Young modulus elastomeric stamps are particularly advisable for texturing nanocomposites, whose surface roughness can be substantially increased by the incorporated nanocrystals and their possible aggregates, hence requiring remarkable short-scale ($<10\,\mu m$)[12] conformability of the moulds to obtain effective pattern transfer. The composite starts to wet the lateral walls of the recessed features in the mould up a filled height depending on the heating time (Fig. 2b, c). Afterwards, the system is driven below the matrix glass transition temperature (T_g), and the mould is detached from the surface (Fig. 2d), which turns out to be textured with the same pattern

[*] Dr. D. Pisignano,[+] Dr. L. Persano, S. Molle, S. Girardo, Dr. A. A. R. Neves, Dr. A. Camposeo, R. Stabile, Prof. R. Cingolani
NNL, National Nanotechnology Laboratory of Instituto Nazionale di Fisica della Materia-Consiglio
Nazionale delle Ricerche, c/o Distretto Tecnologico ISUFI
via Arnesano, I-73100 Lecce (Italy)
E-mail: luana.persano@unile.it

[+] Present address: Istituto Superiore di Formazione Interdisciplinare (ISUFI), Università del Salento, Lecce (Italy)

[**] We gratefully acknowledge the financial support from the Regional Strategic Project 'Ponamat', from the Italian Institute of Technology, and from the Italian Ministry of University and Research through the FIRB project RBIP06SH3W.

ADVANCED FUNCTIONAL MATERIALS

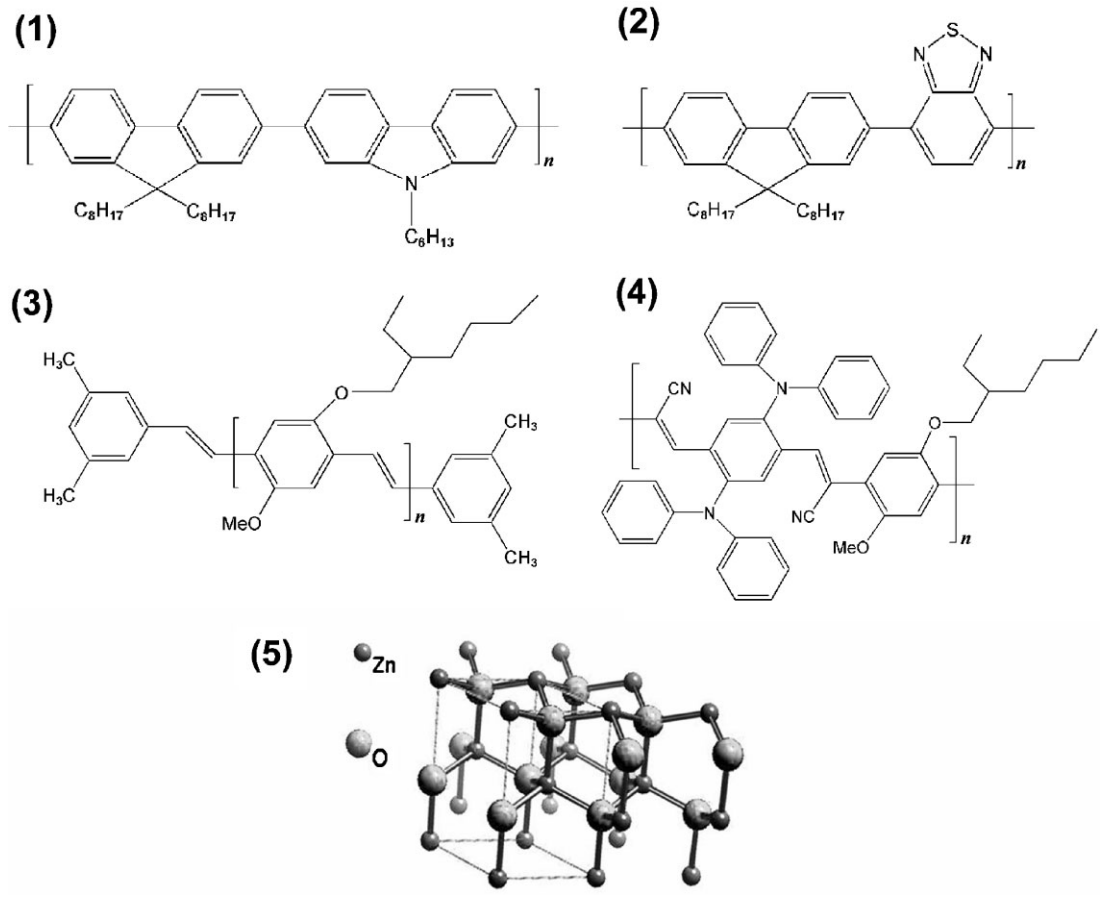

Figure 1. Molecular structures of conjugated polymers employed in light-emitting nanocomposites: (**1**) poly[(9,9-dioctylfl uorenyl-2,7-diyl)-alt-*co*-(9-hexyl-3,6-carbazole)], (**2**) poly[(9,9-dioctylfluorenyl-2,7-diyl)-*co*-(1,4-benzo-{2,1′,3}-thiadiazole)], (**3**) MEH-PPV and (**4**) poly{[2-methoxy-5-(2-ethylhexyloxy)-1,4-(1-cyanovinylenephenylene)]-*co*-[2,5-bis(*N*,*N*′-diphenylamino)-1,4-phenylene]} and ZnO crystal structure (**5**, smaller dots = Zn atoms, larger dots = O atoms).

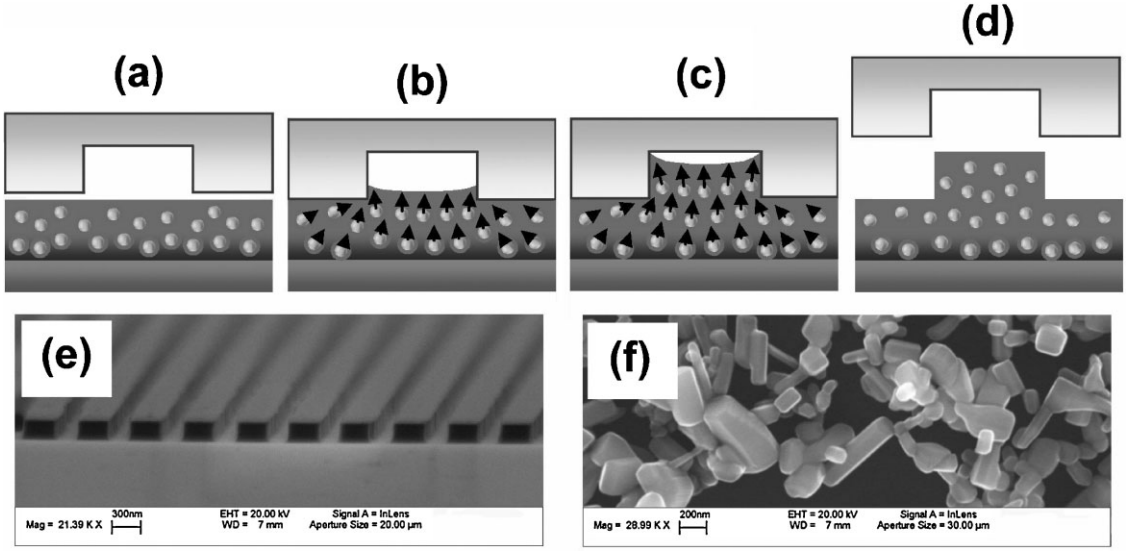

Figure 2. a)–d) Schematic diagram of SM process on nanocomposites (features not in scale). a) Mould-composite contact, b) heating above softening temperature, c) capillarity driven nanofluidic filling, d) cooling down to room temperature and mould separation. e) Cross-sectional view of a 560 nm-period master template. f) Employed ZnO nanoparticles imaged by SEM.

as the starting master template [scanning electron microscopy (SEM) picture displayed in Fig. 2e]. Our transferred patterns include gratings with period (Λ) between 500 nm and a few micrometres, on nanocomposites embedding ZnO particles of size in the range of 100–600 nm (Fig. 2f).

In SM, the vertical transport of the composite relies on capillarity effects undergone by the polymer component, the main driving force being the Laplace pressure, $P_L = 2\gamma\cos\Theta/R$, where γ, Θ and R indicate the fluid–air surface tension, the contact angle between the liquid and the surface of the micro- or nanochannels given by the recessed mould features, and the hydraulic radius of the capillary, respectively. In the simplified case of viscous forces predominant over inertial forces and of laminar flow for Newtonian melts,[13] the time required to fill the voids of mould up to the height, z, is given by the following equation:[9]

$$t = \frac{2\eta z^2}{\gamma R \cos\theta} \quad (1)$$

where η indicates the viscosity of the rising composite. The Poiseuille flow is therefore strongly affected by η. As in many organic materials the viscosity above T_g exhibits a dramatic decrease because of the increased molecular mobility,[14] the increase in temperature is effectively exploited in SM to allow the filling of the pattern in a few minutes. However, since the presence of incorporated particles can significantly disfavour the micro- or nanofluidic molecular flow, longer heating intervals (up to two to three times) and higher temperatures (by about 50 °C) are required for SM on composites with respect to the corresponding purely polymeric materials, as we find for all our investigated systems. The choice of the processing temperature is particularly critical in the case of light-emitting nanocomposites, since, while low temperatures can cause incomplete or too slow capillary penetration, excess heating may lead to (i) very low viscosity of the organic component, thus not being able to vertically carry inorganic nanoparticles and (ii) full, irreversible degradation of the luminescence properties mainly induced by oxygen incorporation and substitution[15] during high-temperature soft lithography. For the optimal choice of the process parameters, an in-depth assessment of the rheological behaviour of the nanocomposite films is therefore particularly important.

For this reason, we analyse the thermo-mechanical response of the prototypical light-emitting blend, poly[2-methoxy-5-(2-ethylhexyloxy)-1,4-phenylene-vinylene] (MEH-PPV)/poly (methylmethacrylate) (PMMA) and of its composite with ZnO particles. Figure 3 displays the dynamic storage (G') and loss (G'') moduli (a) of PMMA, (b) of the polymeric blend and (c) of the nanocomposite, respectively, measured at 170 °C for frequencies (ω) consistent with the values of shear-rates of viscous systems at the entrance of micro- or nanochannels.[16] A transition from solid-like ($G' > G''$) to liquid-like ($G' < G''$) behaviour is clearly appreciable from the intersection of the

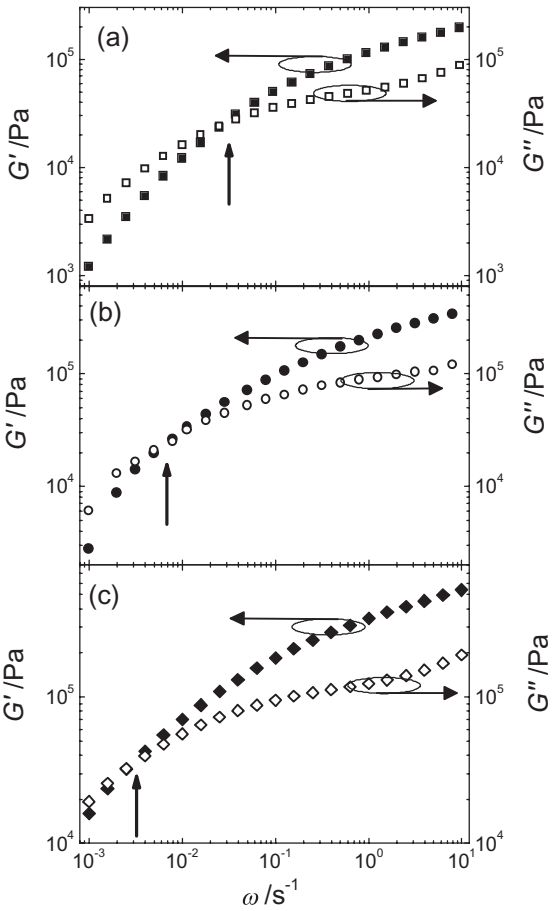

Figure 3. Storage modulus, G' (full symbols, left vertical scale), and loss modulus, G'' (empty symbols, right scale) versus frequency, ω, for PMMA a), MEH-PPV/PMMA b), and ZnO nanocomposite c).

linear viscoelastic moduli upon decreasing ω, with crossover frequency, ω_c (for which G' equals G'') of 3×10^{-2}, 6×10^{-3} and $3 \times 10^{-3}\,s^{-1}$ for the PMMA, the polymeric blend and the nanocomposite, respectively. Therefore, the inclusion of inorganic nanoparticles in the polymer matrix doubles the longest relaxation time ($\tau = \omega_c^{-1}$)[17a] in the system, moreover increasing the absolute values of the elastic modulus, and decreases the slope of the G' and G'' curves (Fig. 3b and c). A similar behaviour is observed in a number of composite systems such as fluoroelastomers[17a] and thermoplastics[17b–f] incorporating organoclays, and concentrated suspensions of hard spheres,[17g] and attributed to the reduction of local mobility of polymeric chains as consequence of strong filler–polymer interactions resulting in physically networked structures, or in shear-induced supramolecular orientation. The system viscosity is enhanced upon addition of the nanocrystals as well (Fig. 4). With respect to PMMA, η is more than four times larger in the nanocomposite including ZnO particles, which provided resistance to melt flow and deformations. Furthermore, the ratio of the lost to stored energy, $\tan\delta = G''/G'$ is decreased by the inclusion of inorganic fillers in the polymeric blends (inset of Fig. 4), which is related to an

ADVANCED FUNCTIONAL MATERIALS

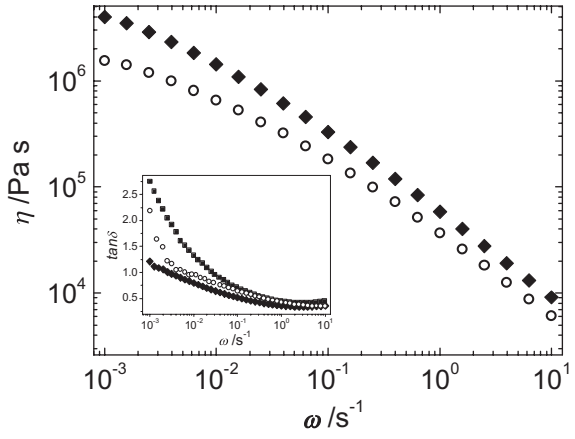

Figure 4. Frequency dependence of viscosity, η, of PMMA (full squares), MEH-PPV/PMMA (empty circles) and ZnO nanocomposite (full diamonds). Inset: frequency dependence of the dissipation coefficient, tan δ, for the three materials (same used symbols).

enhancement of the elastic, solid-like character of the material. However, a shear-thinning behaviour is appreciable in all the investigated range of ω (Fig. 4), and particularly for the composite system, from which high-temperature patterning of the nanocomposites can benefit.[17c] In particular, since SM heating must be longer than the characteristic time-scale of structural rearrangement of the melt, the composite material has to be kept at high temperature for longer times (15 instead of 5 min) to allow its terminal flow to determine the irreversible deformation and hence the pattern transfer from the mould.

This is shown in Figure 5, displaying the micrographs of gratings with $\Lambda = 4\,\mu$m on the mould template (bright field image in Fig. 5a) and on printed nanocomposites of ZnO particles embedded in the four light-emitting polymers, **1**–**4** (fluorescence images in Fig. 5b–e, respectively). The good fidelity of the mould and the large patterned area are appreciable from the comparison of Figure 5a and b–e. In particular, the obtained periodicity faithfully reproduces that of the mould, and the two dimensional view and the cross-section of the final nanocomposite gratings, imaged by atomic force microscopy (AFM) in Figure 5f and g, show a well-defined pattern, clearly indicating that the achievable resolution can be further reduced, depending on the starting master. A direct comparison between a master with $\Lambda = 560$ nm, fabricated by electron-beam lithography (EBL), and the resulting nanocomposite pattern allows one to appreciate that the final periodicity and width of the features replicate those of the template with good fidelity even in the sub-μm scale (Fig. 6). An aspect-ratio loss of the order of 20% with respect to the master is observable in the printed sample because of an incomplete filling of the recessed features of the mould, which can be reduced by increasing the heating interval during SM or by slightly decreasing the nanoparticles amount in the composite film. The minor topographic inhomogeneities observable in the AFM images of the nanocomposites correspond to the regions of luminescence contrast due to

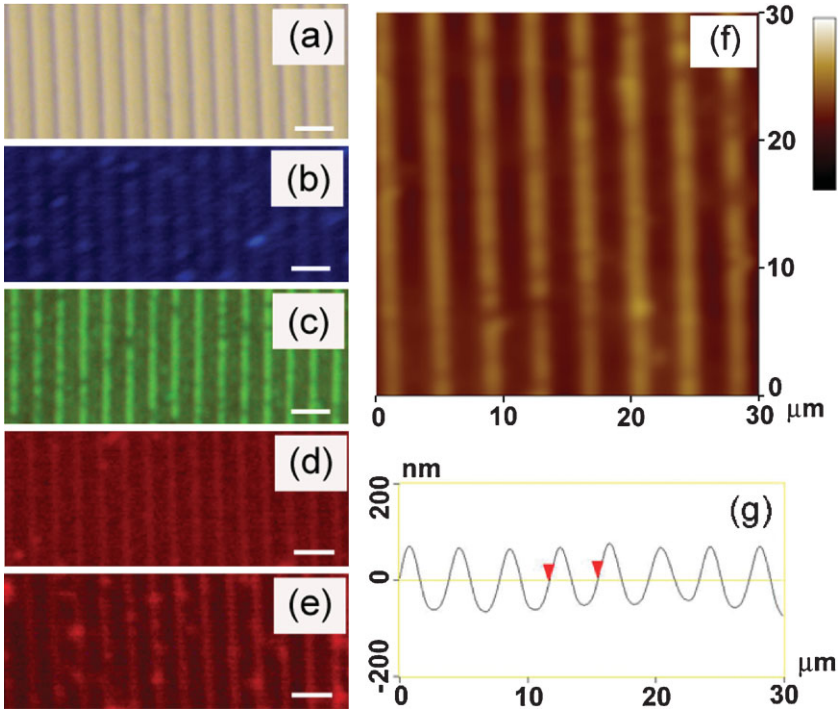

Figure 5. Bright field optical micrograph of 4 μm-period mould a), and corresponding SM pattern transfer to nanocomposites of ZnO and conjugated polymers (1–4), imaged by fluorescence microscopy (b–e, respectively). Marker = 5 μm. e) AFM two-dimensional view of the nanocomposite grating. f) Corresponding cross-section. Vertical scale from zero to 500 nm.

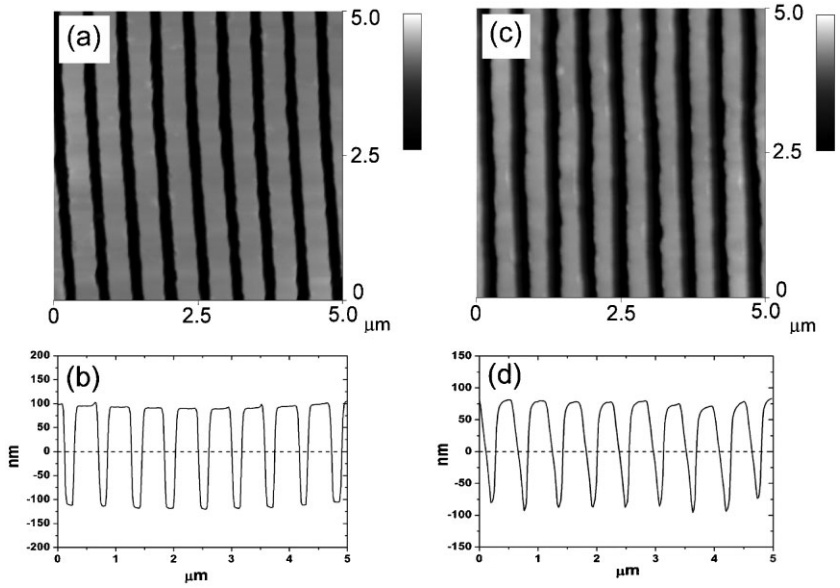

Figure 6. AFM view of a 560 nm-period master a), vertical scale from zero to 300 nm, and master cross-sectional profile b), together with the corresponding patterned nanocomposite with MEH-PPV c) vertical scale from zero to 200 nm and resulting cross-section d). Typical patterned features in experiments with this master exhibit height from 15 to 20 to more than 160 nm, and full width at half maximum of about 400 nm, faithfully replicating the width of the master features.

local microscale aggregations of particles, analogously with experiments on patterning of nanocrystals films.[5f]

In order to assess the retained luminescence properties of patterned nanocomposites, we collected the photoluminescence (PL) spectra before and after the lithography process (Fig. 7), and investigated for the first time the PL efficiency, Φ, achievable with nanocrystals-conjugated polymer donor-acceptor systems. For all the studied composites, the integrated PL spectra show slight variation in the emission peak wavelength, λ ($\leq$5%), and a change of the full width at half maximum, $\Delta\lambda$, up to 40% (Table 1). In some light-emitting polymers, excited by the embedded inorganic particles via non-radiative energy transfer, the spectra exhibit an enhancement of the low-energy vibronic replicas or tails, suggesting oxidative reduction of the conjugation length or excitonic migration and relaxation to excimer species.[18] Nonetheless, the absolute quantum yield after SM is still generally larger than 10–15% for all the composites, whose figure of merit is fully valid for the eventual realization of nanopatterned light-emitting devices (Table 1).[19]

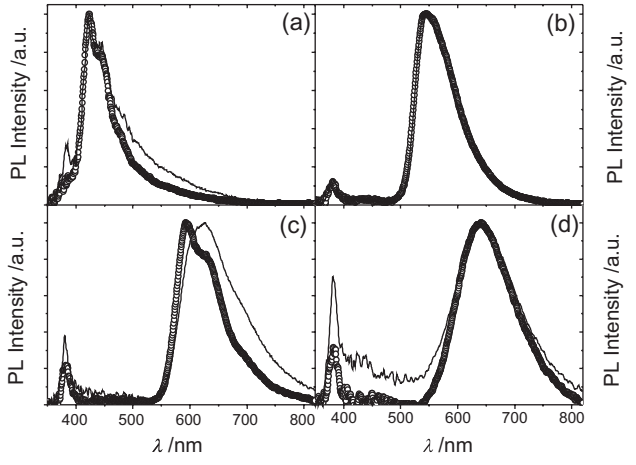

Figure 7. Integrated PL spectra before (empty circles) and after (superimposed lines) SM nanopatterning. From a) to d), spectra correspond to nanocomposites with polymers from **1** to **4**, respectively.

To this aim, we study the effect of patterned gratings on the directionality of light emitted from the nanocomposites. The angle-resolved PL spectra of a film with ZnO particles and MEH-PPV structured with a 560 nm period grating are shown in Figure 8. The presence of the periodic corrugation in the nanocomposite enhances the light emitted towards certain forward angles (Ψ), due to the printed, one-dimensional wavelength-scale periodicity. In such linear distributed feedback microcavities, the angle-dependent emission wavelength, λ_Ψ, relates to the effective refractive index of the waveguide mode, n_{eff}, and to the diffraction order inside the luminescent slab according to the conservation of the in-plane component of the wave vector of the emitted light.[20] By this relation, we

Table 1. Emission spectral properties, peak wavelength (λ) and full width at half maximum ($\Delta\lambda$) and PL quantum yields (Φ) of the nanocomposites, before and after SM.

Composite	Before SM			After SM		
	λ [nm]	$\Delta\lambda$ [nm]	Φ	λ [nm]	$\Delta\lambda$ [nm]	Φ
1	423	52	46 ± 4	423	63	24 ± 6
2	545	82	92 ± 3	543	79	72 ± 7
3	593	87	35 ± 4	627	119	17 ± 4
4	641	115	29 ± 1	648	129	20 ± 6

ADVANCED FUNCTIONAL MATERIALS

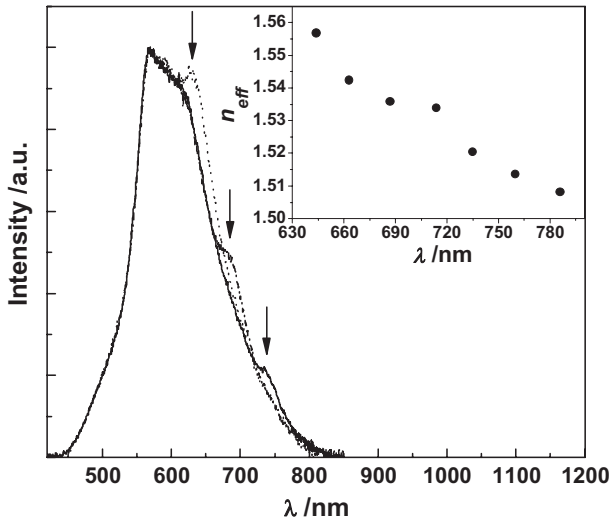

Figure 8. a): PL spectra from a 560 nm-period patterned nanocomposite (with MEH-PPV), at collection angle: 12° (solid line), 18° (dashed line) and 24° (dotted line). The vertical arrows evidence the angular dependence of the emission peaks induced by the imprinted grating. Inset: wavelength dependence of n_{eff}.

estimate the wavelength dependence of n_{eff} of the nanostructured light-emitting composite, which decreases from 1.56 to 1.51 upon increasing λ_Ψ from 644 to 786 nm (inset of Fig. 8).

The specific advantages of this approach over other technologies for patterning nanocomposites[6–8] are numerous. The SM is not affected by multiple reflections, scattering, and in situ diffraction due to embedded nanoparticles,[7a] which, besides well-know mask diffraction effects, can limit the resolution and the exposure homogeneity achievable with optical methods when applied to nano-scale heterogeneous materials. The method is parallel, and cheap as it does not need any exposure or pressing set-up. In SM, the penetration of the polymer into the recessed features of the mould is driven by capillarity effects, thus being marginally affected by problems of difficult polymer transport, which can be relevant under the pressure applied by hard moulds during nanoimprinting, and further enhanced by the presence of nanoparticles suppressing the molecule flow,[21] as here demonstrated. Concomitantly, SM is immune from pattern shrinkage or distortions, induced by the solvents employed by other soft lithography techniques. We believe that a more controlled atmosphere for film preparation and processing can lead to an even better preservation of the optical properties of light-emitting composites, with respect to the here reported results.

3. Conclusions

We demonstrate structuring of light-emitting nanocomposite materials including ZnO particles and conjugated polymers, with resolution up to wavelength-scale. The SM technology allows one to overcome the flow difficulties induced by embedding nanocrystals in polymer compounds. These results open new possibilities for the realization of nanopatterned devices based on hybrid organic-inorganic systems. Texturing composites with high (sub-500 nm) spatial resolution will enable tailoring the device emission resulting from donor–acceptor energy transfer by lithographic filtering of the nanoparticles able to penetrate in the mould template by vertical nanofluidics.

4. Experimental

Materials: For the preparation of the nanocomposites, the following light-emitting conjugated polymers were used, purchased from American Dye Source Inc. (Quebec, Canada): (**1**) poly[(9,9-dioctylfluorenyl-2,7-diyl)-alt-*co*-(9-hexyl-3,6-carbazole)], (**2**) poly[(9,9-dioctylfluorenyl-2,7-diyl)-*co*-(1,4-benzo-{2,1′,3}-thiadiazole)], (**3**) MEH-PPV and (**4**) poly{[2-methoxy-5-(2-ethylhexyloxy)-1,4-(1-cyanovinylene-phenylene)]-*co*-[2,5-bis(*N*,*N*′-diphenylamino)-1,4-phenylene]}. Zinc oxide particles were purchased by Sigma–Aldrich, Inc. PMMA (Sigma–Aldrich) was also employed as blending component in the composites aiming to increase the radiative decay efficiency by reducing the formation of nonradiative recombination centres in the conjugated polymers and to improve the overall photostability[5h]. Solutions were prepared by dispersing polymers and ZnO particles in toluene (J.T. Baker, Phillipsburg, NJ), with relative concentrations (ZnO/conjugated polymer) between 3:2 and 1:4 in weight. PDMS (Sylgard 184, Dow Corning, Midland, MI, USA), trimethylsiloxy-terminated vinylmethylsiloxane-dimethylsiloxane (VDT-731, ABCR, Karlsruhe, Germany), platinum divinyltetramethyldisiloxane (ABCR), 2,4,6,8-tetramethyltetravinylcyclotetrasiloxane (Sigma–Aldrich) and methylhydrosiloxane-dimethylsiloxane (HMS-301, ABCR) were used for the realization of elastomeric moulds.

Lithography: A set of master structures made by parallel stripes with period ranging from 560 nm to 4 μm was fabricated. Sub-micrometre period gratings were obtained by EBL on silicon wafers, performed with a Raith 150 system at an acceleration energy of 20 KeV, lift-off and subsequent reactive ion etching by a CF_4/Ar mixture. Micrometre-scale masters were realized by optical lithography on Si/SiO_2 substrates, with an EVG 620 mask aligner. After the deposition of standard photoresist, UV-exposure and development, we etched the thermal dioxide by using $NH_4F/HF/H_2O$ (6.6 g:1.6 mL:10 mL). The so obtained SiO_2 mask was then employed to etch Silicon by 5.9 M solutions of KOH at 80 °C. PDMS and *h*-PDMS moulds were then obtained from the masters according to standard procedures [10]. Nanocomposite films were spin-cast onto cleaned quartz substrates from the toluene solutions, at 1600 rpm for 60 s, providing a uniform film thickness of about 350 nm. SM was carried out by placing the moulds on the composite films under their own weight, and heating the samples at 170 °C in glove-box nitrogen atmosphere (oxygen ppm < 10), for about 15 min. Generally, PDMS moulds led to better patterning results due to higher conformability to local surface dishomogeneities in the nanocomposite films.

Rheological Characterization: Rheological measurements were carried out by a rotational rheometer (TA Instruments Inc., New Castle, DE, USA). Samples of PMMA, MEH-PPV/PMMA and composites including ZnO particles with relative concentration of 60% with respect to MEH-PPV were prepared as disks of 1 mm thickness and 25 mm diameter. They were studied using a parallel plate geometry, at $T = 170$ °C under nitrogen atmosphere. The linear viscoelasticity region for the investigated materials was determinated by amplitude sweep experiments.

AFM Characterization: The morphological characterization of the nanopatterned surfaces was carried out by tapping AFM in air, by using a Nanoscope III controller with a Digital Instruments Multimode head,

integrated with a J-scanner (maximum scan size of $90 \times 90\,\mu m^2$). Phosphorous-doped Si tips were employed with an 8–10 nm nominal curvature radius and a resonant frequency of 160 and 280 kHz.

Optical Measurements: Fluorescence micrographs of the nanocomposite gratings were collected by a Leica MZ16FA stereomicroscope coupled to a 3264×2448 pixels camera (Leica DFC490), under excitation by a Hg lamp. The PL spectra of the nanocomposite films before and after patterning were measured by a fiber-coupled monochromator (TRIAX 320, Jobin Yvon), equipped with a charge coupled device (Jobin Yvon), and exciting the materials with a He–Cd laser ($\lambda = 325$ nm). Angle-resolved PL measurements were carried out by collecting photons emitted in a small solid angle ($\cong 10^{-3}$ rad) around each value of the collection angle (Ψ), measured by moving in the plane perpendicular to the nanopatterned grooves. The luminescence absolute quantum efficiency (Φ) was measured by determining the number of PL photons emitted per absorbed photon, placing samples in an integrating sphere, and accounting for the excitation light which is not absorbed by the sample at its first incidence, and is absorbed after successive reflections on the reflecting sphere surface [19]:

$$\Phi = \frac{P_1 - (R+T)P_2}{(1-R-T)X_L} \tag{2}$$

In the previous expression, R and T indicate the sample reflectance and transmittance, respectively, P_1 and P_2 are the PL signals measured with the laser beam incident on the sample and on the integrating sphere, respectively, and X_L stands for the excitation signal, measured with the laser incident on the sphere and without sample. All the optical measurements were carried out at room temperature.

Received: February 18, 2008
Revised: May 26, 2008
Published online: September 1, 2008

[1] a) C. Sanchez, B. Lebeau, F. Chaput, J. P. Boilot, *Adv. Mater.* **2003**, *15*, 1969. b) A. Maity, M. Biswas, *J. Ind. Eng. Chem.* **2006**, *12*, 311. c) A. C. Balazs, T. Emrick, T. P. Russell, *Science* **2006**, *314*, 1107.

[2] G. M. Russo, G. P. Simon, L. Incarnato, *Macromolecules* **2006**, *39*, 3855.

[3] R. Gangopadhyay, A. De, *Chem. Mater.* **2000**, *12*, 608.

[4] K. Esumi, H. Houdatsu, T. Yoshimura, *Langmuir* **2004**, *20*, 2536.

[5] a) V. L. Colvin, M. C. Schlamp, A. P. Alivisatos, *Nature* **1994**, *370*, 354. b) W. Caseri, *Macromol. Rapid Commun.* **2000**, *21*, 705. c) N. Tessler, V. Medvedev, M. Kazes, S. Kan, U. Banin, *Science* **2002**, *295*, 1506. d) W. H. Huynh, J. J. Dittmer, A. P. Alivisatos, *Science* **2002**, *295*, 2425. e) L. Bakueva, S. Musikhin, M. A. Hines, T.-W. F. Chang, M. Tzolov, G. D. Scholes, E. H. Sargent, *Appl. Phys. Lett.* **2003**, *82*, 2895. f) Y. Wang, Z. Tang, M. A. Correa-Duarte, L. M. Liz-Marzán, N. A. Kotov, *J. Am. Chem. Soc.* **2003**, *125*, 2830. g) J. H. Park, Y. T. Lim, O. O. Park, J. K. Kim, J.-W. Yu, Y. C. Kim, *Chem. Mater.* **2004**, *16*, 688. h) N. Cho, K. R. Choudhury, R. B. Thapa, Y. Sahoo, T. Ohulchanskyy, A. N. Cartwright, K. S. Lee, P. N. Prasad, *Adv. Mater.* **2007**, *19*, 232. i) A. A. R. Neves, A. Camposeo, R. Cingolani, D. Pisignano, *Adv. Funct. Mater.* **2008**, *18*, 751.

[6] L. Pang, Y. Shen, K. Tetz, Y. Fainman, *Opt. Express* **2005**, *13*, 44.

[7] a) C. Ingrosso, V. Fakhfouri, M. Striccoli, A. Agostiano, A. Voigt, G. Gruetzner, M. L. Curri, J. Brugger, *Adv. Funct. Mater.* **2007**, *17*, 2009. b) C. Paquet, E. Kumacheva, *Adv. Funct. Mater.* **2007**, *17*, 3105.

[8] a) V. C. Sundar, H. J. Eisler, T. Deng, Y. T. Chan, E. L. Thomas, M. G. Bawendi, *Adv. Mater.* **2004**, *16*, 2137. b) M. Tamborra, M. Striccoli, M. L. Curri, J. A. Alducin, D. Mecerreyes, J. A. Pomposo, N. Kehagias, V. Reboud, C. M. Sotomayor Torres, A. Agostiano, *Small* **2007**, *3*, 822. c) V. Reboud, N. Kehagias, C. M. Sotomayor Torres, M. Zelsmann, M. Striccoli, M. L. Curri, A. Agostiano, M. Tamborra, M. Fink, F. Reuther, G. Gruetzner, *Appl. Phys. Lett.* **2007**, *90*, 011115.

[9] a) K. Y. Suh, Y. S. Kim, H. H. Lee, *Adv. Mater.* **2001**, *13*, 1386. b) D. Pisignano, L. Persano, G. Gigli, R. Cingolani, F. Babudri, G. M. Farinola, F. Naso, *Appl. Phys. Lett.* **2004**, *84*, 1365.

[10] a) Y. Xia, G. M. Whitesides, *Angew. Chem.* **1998**, *37*, 550. b) H. Schmid, B. Michel, *Macromolecules* **2000**, *33*, 3042.

[11] S. Y. Chou, P. R. Krauss, P. J. Renstrom, *Science* **1996**, *272*, 85.

[12] A. Bietsch, B. Michel, *J. Appl. Phys.* **2000**, *88*, 4310.

[13] T. M. Squires, S. R. Quake, *Rev. Mod. Phys.* **2005**, *77*, 977.

[14] a) H. Vogel, *Phys. Z* **1921**, *22*, 645. b) G. S. Fulcher, *J. Am. Ceram. Soc.* **1925**, *8*, 339. c) G. Tamman, W. Hesse, *Z. Anorg. Allg. Chem.* **1926**, *156*, 245. d) K. L. Ngai, D. J. Plazek, *Physical Properties of Polymers Handbook* (Ed: J. E. Mark), American Institute of Physics Press, Woodbury, New York **1996**, pp. 72–152.

[15] M. Yan, L. J. Rothberg, F. Papadimitrakopoulos, M. E. Galvin, T. M. Miller, *Phys. Rev. Lett.* **1994**, *73*, 744.

[16] As low-viscosity prepolymers (i.e. with $\eta \cong 0.15$ Pa s) typically exhibit penetration speed, dz/dt, of the order of 10^2–$10^3\,\mu m\,s^{-1}$ at the entrance of 10 μm-wide microchannels see D. Pisignano, F. Di Benedetto, L. Persano, G. Gigli, R. Cingolani, *Langmuir* **2004**, *20*, 4802, corresponding to shear-rates of roughly $(dz/dt)/R = 10$–$10^2\,s^{-1}$, we expect for our more viscous systems ($\eta > 10^3$ Pa s), shear rates well below $10\,s^{-1}$.

[17] a) R. Valsecchi, M. Viganò, M. Levi, S. Turri, *J. Appl. Polym. Sci.* **2006**, *102*, 4484. b) B. Hoffmann, J. Kressler, G. Stöppelmann, C. Friedrich, G.-M. Kim, *Colloid Polym. Sci.* **2000**, *278*, 629. c) H. J. Choi, S. G. Kim, Y. H. Hyun, M. S. Jhon, *Macromol. Rapid Commun.* **2001**, *22*, 320. d) N. Artzi, Y. Nir, M. Narkis, A. Siegmann, *J. Polym. Sci. B: Polym. Phys.* **2002**, *40*, 1741. e) O. Meincke, B. Hoffmann, C. Dietrich, C. Friedrich, *Macromol. Rapid Commun.* **2003**, *204*, 823. f) H. B. Kim, J. S. Choi, C. H. Lee, S. T. Lim, M. S. Jhon, H. J. Choi, *Eur. Polym. J.* **2005**, *41*, 679. g) A. P. Shapiro, R. F. Probstein, *Phys. Rev. Lett.* **1992**, *68*, 1422.

[18] a) T.-Q. Nguyen, B. J. Schwartz, R. D. Schaller, J. C. Johnson, L. F. Lee, L. H. Haber, R. J. Saykally, *J. Phys. Chem. B* **2001**, *105*, 5153. b) J. M. Lupton, M. R. Craig, E. W. Meijer, *Appl. Phys. Lett.* **2002**, *80*, 4489. c) E. J. W. List, R. Guentner, P. Scanducci de Freitas, U. Scherf, *Adv. Mater.* **2002**, *14*, 374.

[19] N. C. Greenham, I. D. W. Samuel, G. R. Hayes, R. T. Phillips, Y. A. R. R. Kessener, S. C. Moratti, A. B. Holmes, R. H. Friend, *Chem. Phys. Lett.* **1995**, *241*, 89.

[20] a) B. J. Matterson, J. M. Lupton, A. F. Safonov, M. G. Salt, W. L. Barnes, I. D. W. Samuel, *Adv. Mater.* **2001**, *13*, 123. b) G. A. Turnbull, P. Andrews, M. J. Jory, W. L. Barnes, I. D. W. Samuel, *Phys. Rev. B* **2001**, *64*, 125122. c) E. Mele, F. Di Benedetto, L. Persano, R. Cingolani, D. Pisignano, *Nano Lett.* **2005**, *5*, 1915.

[21] G. Strobl, *The Physics of Polymers*, Springer, Berlin, Germany **1997**, pp. 192–244.